Ikeda and Tsuji *Progress in Earth and Planetary Science* (2018) 5:62
https://doi.org/10.1186/s40645-018-0211-8

Progress in Earth and Planetary Science

RESEARCH ARTICLE Open Access

Temporal change in seismic velocity associated with an offshore M_W 5.9 Off-Mie earthquake in the Nankai subduction zone from ambient noise cross-correlation

Tatsunori Ikeda[1*] and Takeshi Tsuji[1,2]

Abstract

The Nankai subduction zone off the Kii Peninsula, Japan, has a large potential to generate megathrust earthquakes in the near future. To investigate the temporal variation of stress or strain in the Nankai subduction zone, we estimated the temporal variation of seismic velocity by using cross-correlations of ambient noise in the frequency range 0.7–2.0 Hz, which was dominated by ACR waves, recorded by the DONET offshore seismic network from 1 October 2014 to 30 November 2017. The 1 April 2016 Off-Mie earthquake (M_W 5.9) and its aftershocks occurred beneath the seismic network. Our results document a clear decrease in seismic velocity at the time of the earthquake. These coseismic velocity drops were correlated with peak ground velocities at each station, suggesting that dynamic stress changes due to strong ground motions are a primary factor in coseismic velocity variations. Differences in the sensitivity of seismic velocity changes to peak ground velocity may reflect subsurface conditions at each station, such as geological structures and effective pressure conditions. We also observed a long-term increase in seismic velocities, independent of the 2016 earthquake, that may reflect tectonic strain accumulation around the Nankai subduction zone. After removing the long-term trend, we found that the coseismic velocity drops had not completely recovered by the end of the observation period, possibly indicating nonlinear effects of the 2016 earthquake. Our results suggest that ambient noise cross-correlation might be used to monitor the stress state in the Nankai accretionary prism in offshore environments, which would contribute to a better understanding of earthquake processes.

Keywords: Nankai trough, 2016 Off-Mie earthquake, Monitoring, Ambient noise, Seismic interferometry

Introduction

The Nankai subduction zone, where the Philippine Sea plate is subducting beneath the Japanese Islands at approximately 4.1–6.5 cm/year (Fig. 1; Seno et al. 1993; Miyazaki and Heki 2001), is a well-studied plate convergent margin (e.g., Tobin and Saffer 2009; Moore et al. 2009; Bangs et al. 2009; Park et al. 2010). Damaging great earthquakes in excess of M_W 8 have occurred here every ~ 200 years (Ando 1975) and pose a severe threat to the large cities in this part of Japan. In light of the high seismic risk, geophysical and drilling data have been intensively acquired in the Nankai accretionary prism. Because high pore pressure near a fault acts to reduce the effective stress (which presumably lowers the fault's strength), several studies have used seismic velocity to estimate the pore pressure around seismogenic faults (e.g., Tsuji et al. 2008, 2014; Tobin and Saffer 2009). Shear stress, which is also important to evaluate fault stability, has been evaluated using borehole breakouts (Lin et al. 2010) as well as seismic anisotropy (Tsuji et al. 2011). These studies have found that the direction of maximum horizontal stress changes from perpendicular to the trench seaward of the outer ridge (Fig. 1), to parallel to the trench landward of the outer ridge, to nearly parallel to the direction of plate convergence still further landward (Lin et al. 2010; Chang et al. 2010). These variations in stress orientations have been explained in terms of variations in static stress during the earthquake cycle (Wang and Hu 2006). Therefore,

* Correspondence: ikeda@i2cner.kyushu-u.ac.jp
[1]International Institute for Carbon-Neutral Energy Research (WPI-I2CNER), Kyushu University, Fukuoka 819-0395, Japan
Full list of author information is available at the end of the article

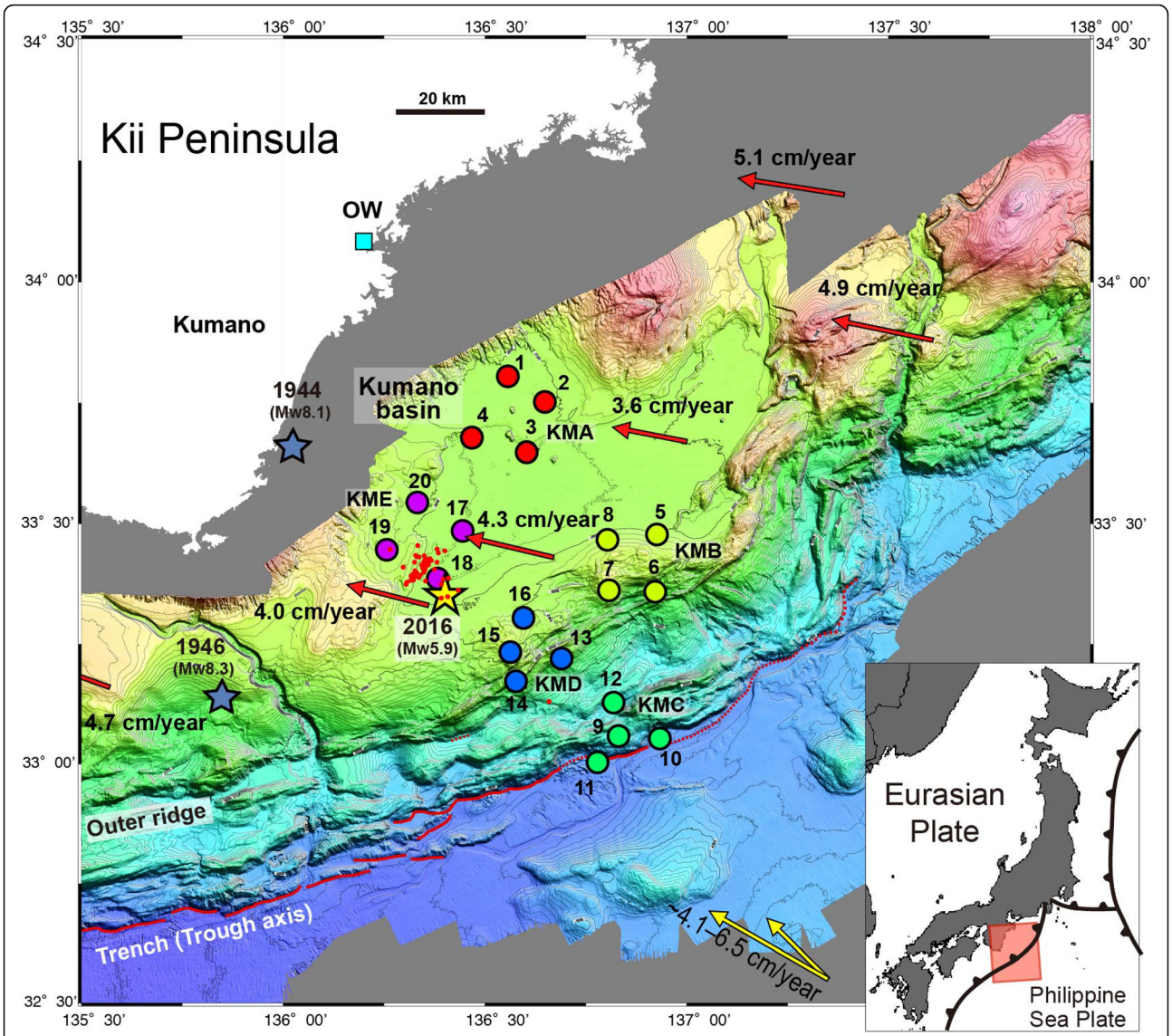

Fig. 1 Tectonic, bathymetric, and geologic features of the Nankai trough region (after Tsuji et al. 2017). Circles represent DONET stations with different colors for each node (KMA, KMB, KMC, KMD, and KME), and the square represents the OW tidal gauge station. The yellow star is the epicenter of the 2016 Off-Mie earthquake, and the red dots represent epicenters of foreshocks and aftershocks from 3 h before to 48 h after the mainshock (Wallace et al. 2016). Blue stars represent the epicenters of the 1944 Tonankai and the 1946 Nankaido earthquakes. Red arrows represent seafloor velocity vectors from Yokota et al. (2016)

determinations of the stress orientation and magnitude should provide useful information for evaluating and monitoring seismogenic faults (e.g., Crampin et al. 2008). As part of that effort, we need to monitor the temporal variation of stress or strain within the accretionary prism.

To monitor seismic activity near the Nankai subduction zone, the Japan Agency for Marine-Earth Science and Technology (JAMSTEC) deployed a network of real-time seafloor observatories off the Kii Peninsula in southwestern Japan called the Dense Oceanfloor Network System for Earthquakes and Tsunamis (DONET) (Kaneda et al. 2015; Kawaguchi et al. 2015). DONET has been used effectively to identify and monitor seismic activity including slow earthquakes such as low-frequency tremors, impulsive low-frequency earthquakes, very low frequency events, and slow slip events, which are important for understanding slip behavior along plate boundary faults (e.g., Nakano et al. 2013, 2014, 2018; Suzuki et al. 2016; Araki et al. 2017; Toh et al. 2018).

On 1 April 2016, the Off-Mie earthquake (M_W 5.9) occurred ~ 50 km off the Kii Peninsula at depth of 11.4 km directly beneath DONET (Wallance et al. 2016; Fig. 1). It was classified as a plate interface event from the analysis of ocean bottom seismometer data, seafloor and

subseafloor geodetic data from DONET, and tsunami modeling (Wallace et al. 2016). This earthquake appears to have ruptured the same plate boundary fault responsible for great interplate earthquakes such as the 1944 Tonankai earthquake (M_W 8.1), although its rupture area was much smaller than that of the 1944 earthquake. Tsuji et al. (2017) showed that the fault planes of the 2016 Off-Mie earthquake and its aftershocks were influenced by the geometry of the plate boundary décollement and the older landward part of the accretionary prism along the coast of the Kii Peninsula. The aftershocks of the 2016 event occurred where the décollement soles onto the top of the oceanic crust beneath the old prism.

Seismic interferometry using ambient noise has been widely used to estimate seismic velocity structures (e.g., Shapiro et al. 2005; Lin et al. 2009; Nakata et al. 2015) and to monitor temporal changes in seismic velocity associated with earthquakes, volcanic activity, and environmental influences (e.g., Brenguier et al. 2008a, 2008b; Obermann et al. 2013, 2014; Nimiya et al. 2017; Wang et al. 2017). For the case of large earthquakes, coseismic and postseismic velocity variations detected by cross-correlation of ambient noise may be related to changes in stress or strain in the subsurface (e.g., Brenguier et al. 2008a; Taira et al. 2015; Hobiger et al. 2016; Nimiya et al. 2017). Tonegawa et al. (2015) used ambient noise cross-correlation to extract virtual seismograms propagating between pairs of stations in the Nankai subduction zone. On the basis of these cross-correlation functions, they inferred the presence of acoustic-coupled Rayleigh (ACR) waves traveling in the ocean and marine sediments, excited by small earthquakes in the Nankai subduction zone.

To investigate temporal changes in stress or strain in the Nankai subduction zone, particularly those associated with the 2016 Off-Mie earthquake, we estimated temporal changes in seismic velocity from cross-correlations of ambient noise. Our results demonstrated that seismic velocity decreased during the 2016 earthquake and increased during the postseismic period. We also observed long-term and short-term variations in seismic velocity that were independent of the 2016 earthquake. In this paper, we discuss possible mechanisms of these seismic velocity variations and implications of our results for understanding future earthquakes.

Data

We used the vertical component of continuous ambient seismic noise recorded by a subset of 20 DONET broadband seismometers (DONET1 hereafter), grouped in five nodes of four seismometers (Fig. 1), from 1 October 2014 to 30 November 2017. Seismic data in the National Research Institute for Earth Science and Disaster Resilience (NIED) data server were not available from node KMD for the period 12 to 31 March 2016, and from node KME for the period 1 October 2014 to 24 March 2015 and after 1 June 2016.

Methods

To extract virtual seismograms propagating between pairs of stations, we computed cross-correlations between two seismic records. We first divided each day of ambient noise data into 30-min segments offset by 15 min (i.e., with 50% overlap). We then applied a band-pass filter in the frequency range 0.7–2.0 Hz, which was dominated by ACR waves in the study area (Tonegawa et al. 2015). To reduce the effects of earthquakes, instrumental irregularities, and non-stationary noise sources on the cross-correlations, we removed segments with root-mean-square (RMS) amplitudes greater than three times the median RMS amplitude of the station or greater than 1.5 times that of adjacent segments. The cross-correlations between stations within each node were computed by power-normalized cross-correlation (cross-coherence) in the frequency domain (e.g., Nakata et al. 2011, 2015).

To estimate temporal changes in seismic velocity from the cross-correlations, we used the stretching interpolation technique (e.g., Sens-Schönfelder and Wegler 2006; Minato et al. 2012; Nimiya et al. 2017). The method elongates the time axis and finds the trace most similar to the reference trace:

$$f_{\varepsilon}^{\mathrm{cur}}(t) = f^{\mathrm{cur}}(t(1+\varepsilon)), \tag{1}$$

$$CC(\varepsilon) = \frac{\int f_{\varepsilon}^{\mathrm{cur}}(t) f^{\mathrm{ref}}(t) dt}{\left(\int \left(f_{\varepsilon}^{\mathrm{cur}}(t)\right)^2 dt \int \left(f^{\mathrm{ref}}(t)\right)^2 dt \right)^{\frac{1}{2}}}, \tag{2}$$

where ε is a stretching parameter, f^{ref} is the reference trace, f^{cur} is the current trace, t is time, and $CC(\varepsilon)$ is the correlation coefficient between the reference and current traces. We applied a grid search algorithm to find the value of ε that maximizes $CC(\varepsilon)$. The parameter ε corresponds to a relative time shift $(\frac{\Delta t}{t})$ and relates to a velocity change $(\frac{\Delta v}{v})$ as follows:

$$\varepsilon = \frac{\Delta t}{t} = -\frac{\Delta v}{v}. \tag{3}$$

The stretching interpolation technique was applied to the coda of cross-correlations, because the coda is more sensitive to velocity changes than the direct wave (e.g., Meier et al. 2010) and less sensitive to variations in noise sources (e.g., Colombi et al. 2014; Chaves and Schwartz 2016). The reference trace was obtained by stacking all available cross-correlations, and the current trace was defined as a 30-day stack of cross-correlations to stabilize the

monitoring results. We selected a window of 30 s for the coda starting 10 s after the arrival of waves with 0.9 km/s apparent velocity. The measured velocity change was considered to represent the velocity change in the middle of the 30-day window. By moving the 30-day window used for the current trace, we estimated the daily variation of the velocity change between pairs of stations in each node. To emphasize seismic velocity changes associated with the 2016 Off-Mie earthquake, we subtracted average values of ε for a 60-day period (18 January to 17 March 2016) before the earthquake (ε_0) from the estimated values of ε as follows:

$$\varepsilon' = \varepsilon - \varepsilon_0. \tag{4}$$

The relative velocity changes $\frac{dv}{v} = -\varepsilon'$ between two stations were estimated by applying the stretching interpolation technique separately for the causal and acausal parts of the cross-correlation codas. To evaluate the standard deviation of $\frac{dv}{v}$, we used the theoretical formula proposed by Weaver et al. (2011) as follows:

$$\sigma_d = \frac{\sqrt{1-CC_{\max}^2}}{2CC_{\max}} \sqrt{\frac{6R}{\omega_c^2(t_2^3 - t_1^3)}}, \tag{5}$$

where t_1 and t_2 are the beginning and end of the time window for the coda, ω_c is the central angular frequency, and $CC_{\max}$ is the maximum correlation coefficient corresponding to the estimated velocity change using Eq. (2). R is the parameter related to the frequency bandwidth (Weaver et al. 2011), and it was calculated by integrating square of auto-correlation of the coda corresponding to the reference trace.

To detect the trend of seismic velocity change at each node, we averaged velocity variations obtained from both causal and acausal parts using all possible station pairs within each node. In averaging, we used the inverse of the square of the standard deviation using Eq. (5) as a weighting factor and calculated the errors by error propagation.

Furthermore, to determine the spatial variation of seismic velocity changes, we applied a simple tomography algorithm in which, assuming that the seismic velocity change between a pair of stations represents the average of the actual velocity changes at each station, we obtained seismic velocity changes at each station by seeking the least-squares solution (Hobiger et al. 2012). We defined velocity changes between a pair of stations from estimates of the both causal and acausal parts of the codas weighted by the inverse of the square of the standard deviation using Eq. (5), which was also used as the weighting factor in the tomography.

Results

Figure 2 shows reference cross-correlations obtained by stacking all available segments in the analyzed period after removing segments based on RMS amplitudes. In the cross-correlations in the northern part of the study area (nodes KMA and KME; Fig. 2a, e), we observed clear seismic waves with group velocities of ~ 1.5 km/s. The signals were stronger when they propagated northward (e.g., from KMA-2 to KMA-1, KMA-3 to KMA-1, and KME-17 to KME-20). Similar features were observed by Tonegawa et al. (2015), who concluded that they were ACR waves traveling in the ocean and marine sediments, persistently excited by small earthquakes near

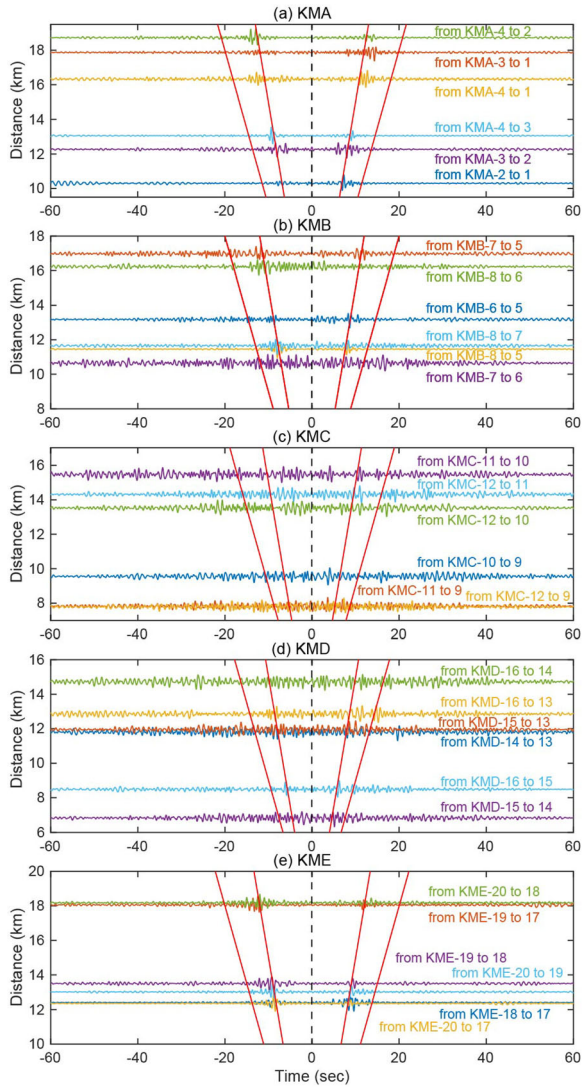

Fig. 2 Reference cross-correlations between station pairs within the five DONET1 nodes. Each node is labeled with the station pair and the propagation direction in positive time. The red lines represent velocities of 0.9 km/s (outer pair) and 1.5 km/s (inner pair). **a** KMA. **b** KMB. **c** KMC. **d** KMD. **e** KME

the Nankai subduction zone. These direct ACR waves were weak in the cross-correlations in the southern part of the study area (nodes KMB, KMC, and KMD; Fig. 2b–d).

By applying the stretching interpolation technique for each set of cross-correlation data, we estimated seismic velocity changes between all possible pairs of stations within each node (Additional file 1). Figure 3 shows examples of temporal variation of cross-correlation data and seismic velocity. We then obtained the average seismic velocity variations at each node (Fig. 4) and velocity variation at each station by using the tomography approach (Fig. 5). These velocity changes clearly decreased at the time of the 2016 Off-Mie earthquake by ~ 0.05 to 0.35% in the averaged velocity changes at each node (Fig. 4). The largest velocity decrease occurred in node KME, the closest node to the epicentral region (Fig. 6; Additional file 2). We observed gradual velocity increases at most of the stations after the earthquake. Before the earthquake, we also observed a long-term variation (gradual increase) and a short-term (several months) fluctuation in the velocity changes (e.g., Fig. 4) that were apparently independent of the 2016 earthquake.

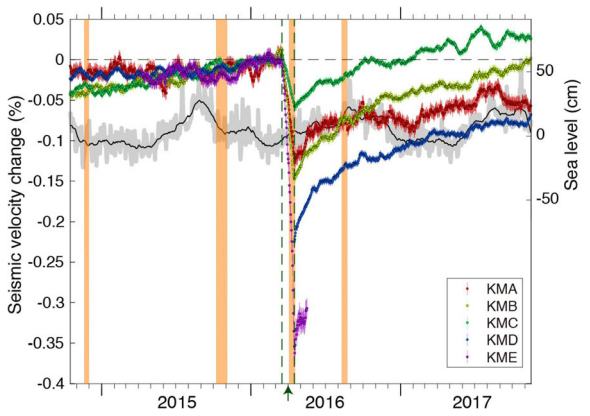

Fig. 4 Temporal variation of the average seismic velocity in each node (colored dots). Error bars correspond to the errors calculated from the standard deviations of seismic velocity change using Eq. (5) by error propagation. The arrow at the bottom indicates the day of the 2016 Off-Mie earthquake, and the vertical dashed lines show the 30-day time window influenced by the mainshock. Gray and black curves represent sea levels at station OW computed by daily and 30-day stacking of hourly data, respectively. Orange areas represent the periods of slow slip events reported by Araki et al. (2017)

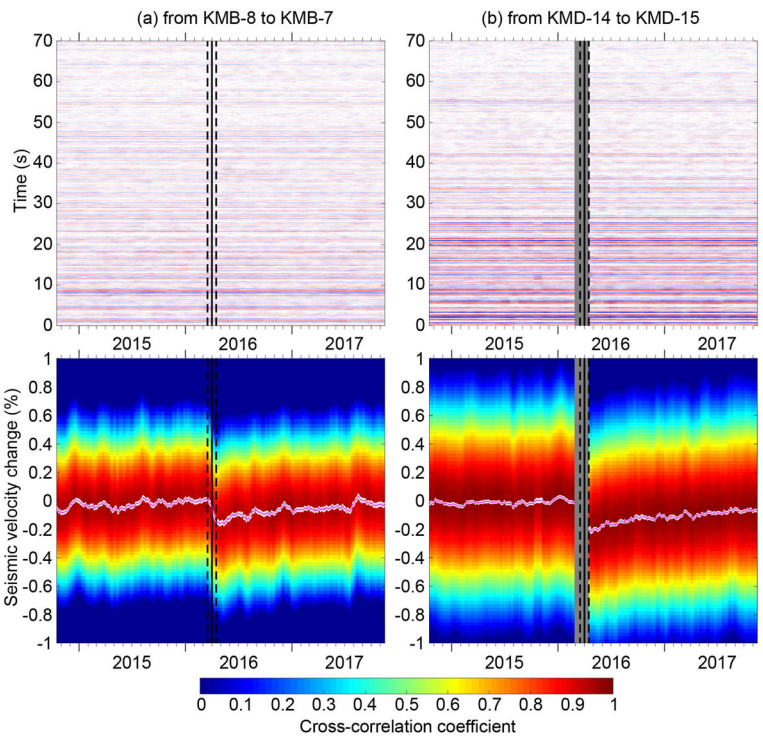

Fig. 3 Examples of temporal variations of cross-correlations and seismic velocities for station pairs. **a** KMB-7 and KMB-8. **b** KMD-14 and KMD-15. Upper plots are daily cross-correlations constructed from the 30-day stacked moving average. Lower plots are seismic velocity variations between two stations obtained from the cross-correlations in the upper panel (thin central magenta line, with standard deviation calculated using Eq. (5), shown in white) with respect to changes before the 2016 Off-Mie earthquake. The background colors indicate the cross-correlation coefficient. Vertical solid lines show the day of the 2016 Off-Mie earthquake and the dashed lines show the 30-day time window influenced by the mainshock. The gray shaded area in **b** represents the set of 30-day periods affected by missing data from node KMD from 12 to 31 March 2016

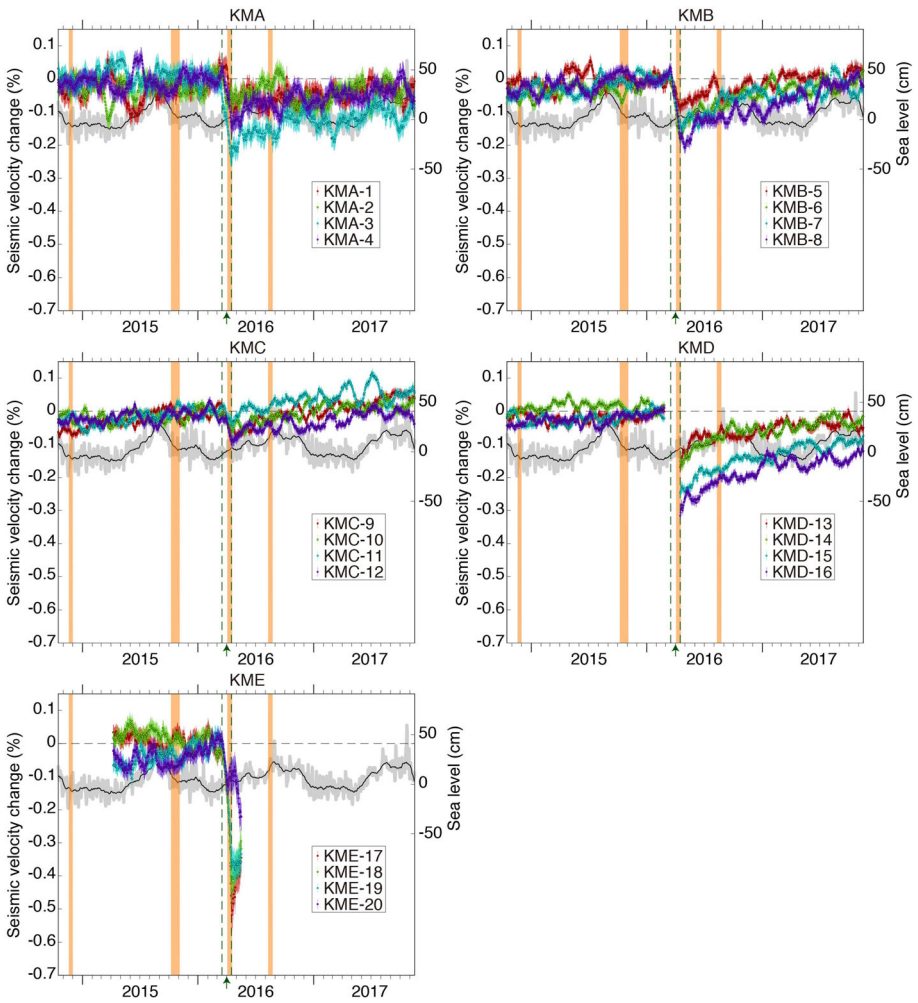

Fig. 5 Temporal variation of seismic velocity at each station (colored dots). Symbols are the same as in Fig. 4

Discussion

Temporal stability and depth sensitivity of coda

In the cross-correlations between pairs of stations, direct ACR waves were not clearly detected in the southern part of the study area (nodes KMB, KMC, and KMD; Fig. 2b–d). This is probably because of the proximity of those stations to the source region of the persistent seismic noises as some of the stations are located in the source region. Nevertheless, we obtained larger values of correlation coefficients through the stretching interpolation in the southern part, indicating that our record of the coda was robust, particularly in the southern part (Additional file 1). The scattering of ACR waves due to the complicated bathymetry and sediment structure in the southern part of study area in Tonegawa et al. (2015) might enhance the directivity of ACR waves and be responsible for the high temporal stability of the cross-correlations.

According to the normal mode calculation of the eigenfunctions of stress (τ_{zz}) by Tonegawa et al. (2015), the stress component (τ_{zz}) of ACR waves propagating in the study area has amplitude (sensitivity) within ocean and marine sediments at 1 Hz. If we assume that the codas of cross-correlations we analyzed were dominated by ACR waves, the estimated velocity changes would be sensitive to a depth of several kilometers below the seafloor as well as in the water layer, although it is difficult to clarify the depth sensitivity because the predicted mode transition is complicated in the studied frequency range (Tonegawa et al. 2015).

Possible mechanism of coseismic velocity change

The opening and closing of cracks due to stress changes are often considered as a mechanism of seismic velocity changes associated with earthquakes. Previous studies have demonstrated that coseismic velocity decreases are correlated with dynamic rather than static changes in stress or strain (e.g., Rubinstein and Beroza 2004; Hobiger et al. 2012, 2016; Brenguier et al. 2014; Taira and

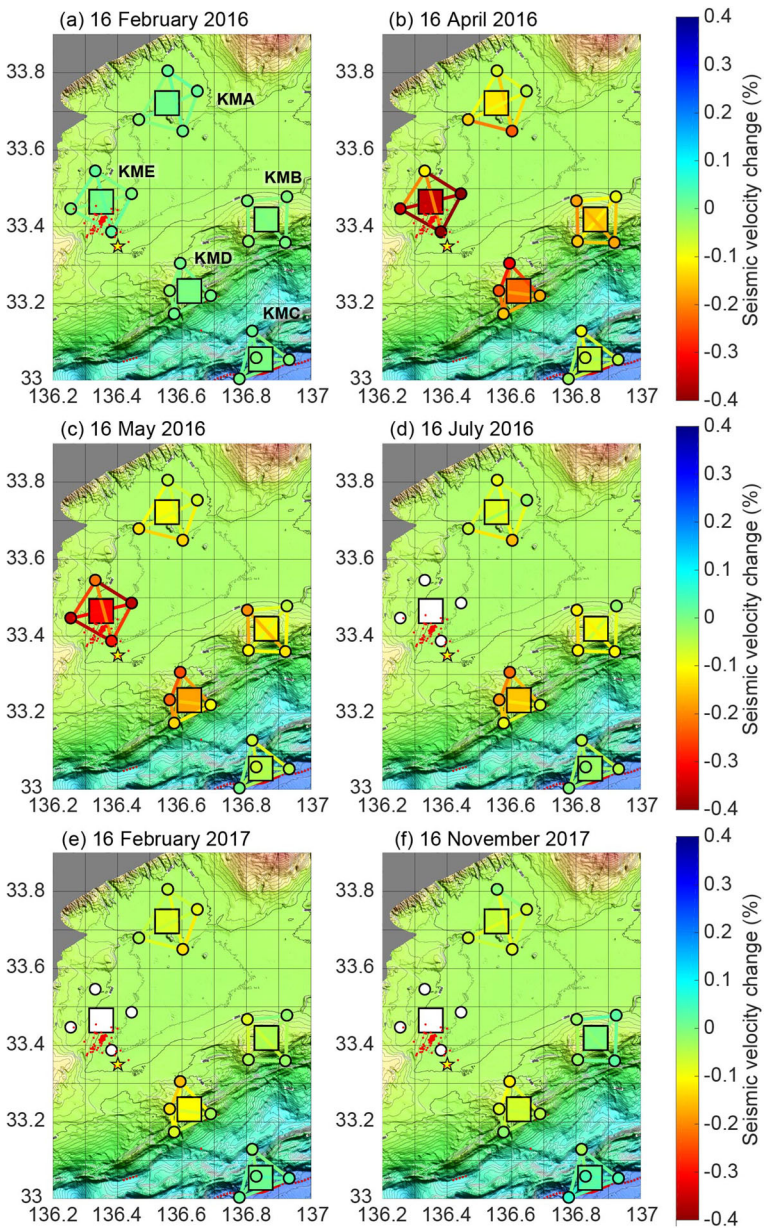

Fig. 6 Snapshots of spatial and temporal seismic velocity variations. Plots show 30-day windows centered on **a** 16 February 2016, **b** 16 April 2016 (including the day of the mainshock), **c** 16 May 2016, **d** 16 July 2016, **e** 16 February 2017, and **f** 16 November 2017. Squares represent the locations of nodes, and their colors represent averaged velocity changes at each node. Circles represent the locations of DONET stations, and their colors represent velocity changes at each station obtained by the tomography approach. Colored lines represent velocity changes between each station pair. The star marks the epicenter of the 2016 Off-Mie earthquake, and red dots are the epicenters of earthquakes in the period from 3 h before to 48 h after the mainshock (Wallace et al. 2016). Additional file 2 presents the complete time series as an animation

Brenguier 2016) and can be explained by the opening and growth of cracks in response to strong ground shaking (e.g., Rubinstein and Beroza 2004; Wu et al. 2009). We therefore compared our estimated coseismic velocity changes at each station with strong ground motion, using peak ground velocity (PGV) as an indicator (Fig. 7). We defined PGV as larger values of PGV of two horizontal components recorded at each station, after bandpass filtering from 0.1 to 10 Hz, by using strong motion data record by DONET1. Seismic velocity changes 15 days after the 2016 earthquake (including the day of the mainshock) at each station were defined as coseismic velocity changes. We observed that the coseismic velocity drops tended to increase with increasing PGV (Fig. 7), which suggests that coseismic velocity changes were influenced by dynamic stress changes due to strong ground shaking.

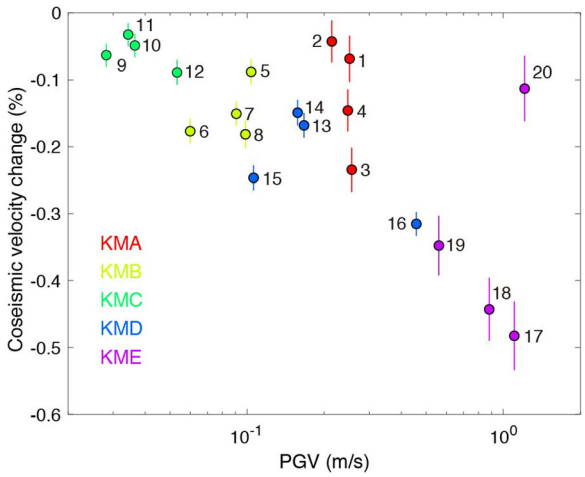

Fig. 7 Comparison between coseismic velocity changes and PGV at each station, denoted by its number. The colors of the station symbols indicate their nodes

The coseismic velocity drops at stations near land (KMA-1, KMA-2, and KME-20) were less sensitive to PGVs than those at other stations. DONET1 stations near land (in nodes KMA and KME) are distributed on the thick sediment deposits of the Kumano basin, whereas other nodes are distributed at the seaward edge of the thin sediments of the Kumano basin or on the accretionary wedge (e.g., Tsuji et al. 2014; Kubo et al. 2018). Such spatial variations in geological structures would reflect scattering in the relationship between coseismic velocity changes and PGVs (Fig. 7). Furthermore, the coseismic velocity changes could be influenced by differences in effective pressure conditions below each station because the sensitivity of seismic velocity to stress change increases as effective pressure decreases (e.g., Toksöz et al. 1976; Zinszner et al. 1997; Shapiro 2003; Brenguier et al. 2014). The high sensitivity of seismic velocity changes to ground shaking might reflect high pore pressures, because fractures are developed around the trough axis (e.g., Kamei et al. 2012; Tsuji et al. 2014, 2015). Because it is difficult to relate our estimated velocity changes to a particular depth, however, comparison of our results with the seismic structure is of limited value.

Curve fitting for observed velocity change

We observed the velocity recovery during the postseismic period as a gradual increase in seismic velocity, except at station KME-20 (Figs. 4 and 5). However, at node KMC (e.g., green line in Fig. 4), the velocity came to exceed its pre-earthquake value approximately 8 months after the earthquake and continued to increase until the end of the study period. Indeed, the seismic velocity variations exhibited a long-term increase before the 2016 earthquake.

Based on the approach by Hobiger et al. (2014, 2016) and Taira et al. (2018), to evaluate the long-term increase and the postseismic velocity change, we fitted the averaged seismic velocity changes at each node $f(T)$ to the following curves.

$$f(T) = A + BT + \left[C + D\exp\left(-\frac{T-T_{\mathrm{eq}}}{E}\right)\right]H\left(T-T_{eq}\right), \quad (6)$$

where T is the day, A, B, C, D, and E are the five fit parameters, $H(T)$ is the Heaviside function, and T_{eq} is the time of occurrence of the Off-Mie earthquake. A is a constant offset, and B is a linear trend of velocity change. C is a non-recovering coseismic velocity change during the observation time, and D is a coseismic velocity change recovering on an exponential scale with time constant E. Linear regressions were applied for the velocity variations before the Off-Mie earthquake to obtain the parameters A and B (Table 1). The parameters C, D, and E were then obtained from the velocity changes after the earthquake through non-linear regressions (Table 1). We did not apply the curve fitting for velocity changes for nodes KMA and KME because the linear trend and the exponential decay in Eq. (6) were difficult to estimate due to large fluctuations, and the data after the earthquake were insufficient for node KME. In both regressions, we used the inverse of the square of the standard deviation as the weight factor and calculated the errors by error propagation.

Long-term increase in seismic velocity

Linear regressions for the average velocity variations at each node yielded velocity increases of 0.013–0.033%/year (Table 1). The 2011 M_W 9.0 Tohoku-Oki earthquake may be partly responsible for the long-term increase in seismic velocity, although the survey area is located ~ 800 km from the epicenter. Coseismic velocity drops and postseismic velocity recovery associated with the 2011 Tohoku-Oki earthquake were widely observed in Japan from cross-correlation of ambient noise using land stations (Hobiger et al. 2016; Wang et al. 2017). If the long-term velocity increase is attributed to postseismic recovery of the Tohoku-Oki earthquake assuming the exponential recovery model, however, the coseismic velocity drops would be much larger than those caused by the Off-Mie earthquake, which we do not expect. We therefore suggest additional factors are required to explain the long-term velocity increase.

Another possible explanation for the long-term increase in seismic velocity is the influence of subduction of the Philippine Sea plate beneath the Eurasian plate (Fig. 1). At land stations in the Tokai region of Japan, a long-term increase in S-wave velocity and a change in

Table 1 Parameters of the best-fitting curves to observed seismic velocity changes. Initial values used in non-linear regression are also listed

Node	B (%/year)	C (%)	D (%)	E (year)
KMB	0.0315 ± 0.0005	− 0.0623 ± 0.0004	− 0.0946 ± 0.0012	0.3249 ± 0.0079
KMC	0.0329 ± 0.0004	− 0.0243 ± 0.0003	− 0.0437 ± 0.0011	0.2770 ± 0.0114
KMD	0.0132 ± 0.0004	− 0.0916 ± 0.0005	− 0.1102 ± 0.0008	0.4559 ± 0.0081
Initial value		− 0.0500	− 0.0500	0.5000

anisotropy, documented by Tsuji et al. (2016) using a continuous controlled seismic source system (e.g., Yamaoka et al. 2008) is consistent with the tectonic strain field of NW-SE compression estimated geodetically by the GNSS Earth Observation Network System. Geodetic observations show that the seafloor around DONET1 is moving 3.6–4.3 cm/year toward the WNW (Fig. 1; Yokota et al. 2016). If this movement continuously generates strain, the increases in seismic velocity that we observed might be used as an indicator of strain accumulation in the Nankai accretionary prism.

The different characteristics of long-term velocity increase at each node could be influenced by local geological structures and stress state. The previous studies using borehole breakouts and seismic anisotropy revealed that the direction of maximum horizontal stress is almost parallel to the direction of plate convergence around DONET1 (Lin et al. 2010; Tsuji et al. 2011). However, the direction of maximum horizontal stress around node KMD is locally perpendicular to the direction of the plate convergence probably reflecting the development of the trough-parallel strike-slip faults in the outer ridge (e.g., Tsuji et al. 2014). The smaller value of the velocity increase rate at node KMD may reflect such spatial variation of stress state and fracture intensity. The long-term velocity increase observed at node KMC directly reflects strain accumulation within the accretionary prism, because node KMC is located on the toe of the accretionary prism where strain accumulation is dominant. On the other hand, nodes KMA and KME are located on the forearc basin above the accretionary prism, thus the long-term velocity increase could be slower, although we had difficulty in estimating a linear trend of velocity increase for nodes KMA and KME due to large fluctuation.

Postseismic velocity recovery

When we removed the long-term increasing trend from the estimated velocity changes by subtracting $A + BT$ from the data, it appeared that the recovery process was not complete at the end of the study period (Fig. 8). The exponential model of Eq. (6) allows us to separate the non-recovering from the recovering coseismic velocity variations (Hobiger et al. 2014, 2016). When we calculated the ratio between the non-recovering coseismic velocity changes C and the total coseismic velocity changes C + D, the non-recovering rates ranged from ~ 35 to 45%, indicating nonlinear effects of the main shock. We note that the non-recovering velocity change means that the velocity changes are not significantly recovering over the observation time, but they are supposed to recover over much longer timescales (Hobiger et al. 2014). The recovery time constants ranged from 0.28 to 0.46 year (Table 1). The non-recovering velocity ratios and the recovery time constants are roughly consistent with the results associated with large earthquakes at land stations in Japan (Hobiger et al. 2014, 2016). However, a detailed comparison with the results using land stations is not straightforward because ACR waves probably dominant in the coda we analyzed would have different frequency-dependent depth sensitivity, compared to those derived from coda of cross-correlation using land stations.

Comparison with sea levels and slow slip events

In addition to the seismic velocity variations mentioned above, we observed a short-term (several months) fluctuation, particularly in DONET1 stations near land (in nodes KMA and KME). The patterns are complicated because they are not correlated with other stations even in the same nodes. Seismic velocity changes measured at land stations

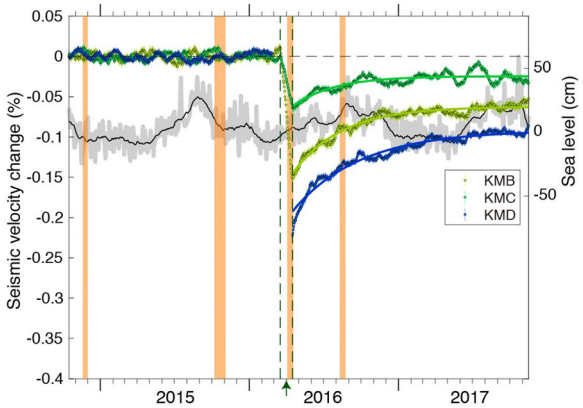

Fig. 8 Temporal variation of average seismic velocity in each node (colored dots) after removing long-term trend. Symbols are the same as in Fig. 4. The solid lines represent the exponential models of Eq. (6) obtained by curve fitting

near the Sea of Japan are strongly correlated with changes in sea level without any remarkable phase shift, probably reflecting an instantaneous elastic response of the lithosphere to ocean loading (Wang et al. 2017). However, the correlation between seismic velocity changes in the DONET1 area and sea level is not clear (Figs. 4, 5, and 8; Additional file 1). Another possible influence on the short-term variation is slow slip events. In their study of slow slip events observed using subseafloor borehole observatories installed in the study area, Araki et al. (2017) reported that eight events accommodated ~ 30–55% (~ 11–22 cm) of the total plate convergence budget (~ 39 cm) from 2011 to 2016. In our results, the estimated seismic velocity changes do not show clear temporal change at the periods of the slow slip events reported by Araki et al. (2017) (orange in Figs. 4, 5, and 8; Additional file 1). We infer that the short-term variation was largely influenced by other factors, such as variations in the sources of ambient noise.

Conclusions

In this study, we estimated temporal changes in the velocity of ACR waves in the Nankai subduction zone by using cross-correlations of ambient noise. Our results showed that drops in seismic velocity were associated with the 2016 Off-Mie earthquake and were followed by post-seismic recovery. The correlation between the coseismic velocity drops and PGVs from the earthquake suggests that the coseismic velocity changes were mainly caused by dynamic stress changes due to strong ground shaking. We also observed a long-term increase in seismic velocity. After removing this long-term trend, our record of velocity changes showed that ~ 35 to 45% of the coseismic velocity drop had not recovered by the end of the study period, suggesting that the mainshock had non-linear effects on velocities. If the long-term increasing trend is related to strain accumulation from plate subduction, our approach may be useful in monitoring variations of the regional stress state, which is difficult to observe in offshore environments, and may provide vital information for understanding future earthquakes.

Additional files

Additional file 1: Temporal variation of seismic velocity and correlation coefficient through stretching interpolation at each station pair. Seismic velocity change and correlation coefficient from causal and acausal parts are displayed, respectively. Symbols are the same as in Fig. 4. (PDF 1981 kb)

Additional file 2: Time sequence of the spatial variations of seismic velocity corresponding to Fig. 6. (MP4 14100 kb)

Abbreviations

ACR waves: Acoustic-coupled Rayleigh waves; DONET: Dense Oceanfloor Network System for Earthquakes and Tsunamis; JAMSTEC: Japan Agency for Marine-Earth Science and Technology; PGV: Peak ground velocity

Acknowledgements

We thank two anonymous reviewers for their constructive comments. We also thank T. Taira for valuable discussions. We used the DONET data obtained from the NIED server (http://www.hinet.bosai.go.jp/?LANG=en). The sea level data at station OW were obtained from the Japan Meteorological Agency (http://www.jma.go.jp/jma/index.html). We used Generic Mapping Tools (Wessel and Smith 1998) for generating Fig. 1. We gratefully acknowledge the support of I2CNER, sponsored by the World Premier International Research Center Initiative, MEXT, Japan.

Funding

This work was supported by the Japan Society for the Promotion of Science through KAKENHI Grant Number 16K18332 and 17H05318, and by the Ministry of Education, Culture, Sports, Science and Technology of Japan (MEXT) through the World Premier International Research Center Initiative.

Availability of data and materials

The DONET data used in this paper are available from the NIED server (http://www.hinet.bosai.go.jp/?LANG=en). The sea level data used in this paper are available from the Japan Meteorological Agency (http://www.jma.go.jp/jma/index.html).

Authors' contributions

TT conceived the study. TI analyzed the data and drafted the manuscript. TT joined in the interpretation and helped to draft the manuscript. Both authors read and approved the final manuscript.

Competing interests

The authors declare that they have no competing interests.

Publisher's Note

Author details

[1]International Institute for Carbon-Neutral Energy Research (WPI-I2CNER), Kyushu University, Fukuoka 819-0395, Japan. [2]Department of Earth Resources Engineering, Kyushu University, Fukuoka 819-0395, Japan.

Received: 22 April 2018 Accepted: 24 August 2018
Published online: 10 October 2018

References

Ando M (1975) Source mechanisms and tectonic significance of historical earthquakes along the Nankai Trough, Japan. Tectonophysics 27:119–140. https://doi.org/10.1016/0040-1951(75)90102-X

Araki E, Safer DM, Kopf AJ, Wallace LM, Kimura T, Machida Y, Ide S, Davis E, IODP Expedition 365 (2017) Recurring and triggered slow-slip events near the trench at the Nankai Trough subduction megathrust. Science 356:1157–1160. https://doi.org/10.1126/science.aan3120

Bangs NLB, Moore GF, Gulick SPS, Pangborn EM, Tobin HJ, Kurumoto S, Taira A (2009) Broad, weak regions of the Nankai Megathrust and implications for shallow coseismic slip. Earth Planet Sci Lett 284:44–49. https://doi.org/10.1016/j.epsl.2009.04.026

Brenguier F, Campillo M, Hadziioannou C, Shapiro NM, Nadeau RM, Larose E (2008a) Postseismic relaxation along the San Andreas fault at Parkfield from continuous seismological observations. Science 321:1478–1481. https://doi.org/10.1126/science.1160943

Brenguier F, Campillo M, Takeda T, Aoki Y, Shapiro NM, Briand X, Emoto K, Miyake H (2014) Mapping pressurized volcanic fluids from induced crustal seismic velocity drops. Science 345:80–82. https://doi.org/10.1126/science.1254073

Brenguier F, Shapiro NM, Campillo M, Ferrazzini V, Duputel Z, Coutant O, Nercessian A (2008b) Towards forecasting volcanic eruptions using seismic noise. Nat Geosci 1:126–130. https://doi.org/10.1038/ngeo104

Chang C, McNeill LC, Moore JC, Lin W, Conin M, Yamada Y (2010) In situ stress state in the Nankai accretionary wedge estimated from borehole wall failures. Geochem Geophys Geosyst 11. https://doi.org/10.1029/2010GC003261

Chaves EJ, Schwartz SY (2016) Monitoring transient changes within overpressured regions of subduction zones using ambient seismic noise. Sci Adv 2:e1501289–e1501289. https://doi.org/10.1126/sciadv.1501289

Colombi A, Chaput J, Brenguier F, Hillers G, Roux P, Campillo M (2014) On the temporal stability of the coda of ambient noise correlations. Comptes Rendus Geosci 346:307–316. https://doi.org/10.1016/j.crte.2014.10.002

Crampin S, Gao Y, Peacock S (2008) Stress-forecasting (not predicting) earthquakes: a paradigm shift. Geology 36:427. https://doi.org/10.1130/G24643A.1

Hobiger M, Wegler U, Shiomi K, Nakahara H (2012) Coseismic and postseismic elastic wave velocity variations caused by the 2008 Iwate-Miyagi Nairiku earthquake, Japan. J Geophys Res Solid Earth 117:1–19. https://doi.org/10.1029/2012JB009402

Hobiger M, Wegler U, Shiomi K, Nakahara H (2014) Signle-station cross-correlation analysis of ambient seismic noise: application to stations in the surroundings of the 2008 Iwate-Miyagi Nairiku earthquake. Geophys J Int 198:90–109. https://doi.org/10.1093/gji/ggu115

Hobiger M, Wegler U, Shiomi K, Nakahara H (2016) Coseismic and post-seismic velocity changes detected by passive image interferometry: comparison of one great and five strong earthquakes in Japan. Geophys J Int 205:1053–1073. https://doi.org/10.1093/gji/ggw066

Kamei R, Pratt RG, Tsuji T (2012) Waveform tomography imaging of a megasplay fault system in the seismogenic Nankai subduction zone. Earth Planet Sci Lett 317–318:343–353. https://doi.org/10.1016/j.epsl.2011.10.042

Kaneda Y, Kawaguchi K, Araki E, Matsumoto H, Nakamura T, Kamiya S, Ariyoshi K, Hori T, Baba T, Takahashi N (2015) Development and application of an advanced ocean floor network system for megathrust earthquakes and tsunamis. In: Seafloor Observatories. Springer Berlin Heidelberg, Berlin, Heidelberg, pp 643–662

Kawaguchi K, Kaneko S, Nishida T, Komine T (2015) Construction of the DONET real-time seafloor observatory for earthquakes and tsunami monitoring. In: Seafloor Observatories. Springer Berlin Heidelberg, Berlin, Heidelberg, pp 211–228

Kubo H, Nakamura T, Suzuki W, Kimura T, Kunugi T, Takahashi N, Aoi S (2018) Site amplification characteristics at Nankai seafloor observation network, DONET1, Japan, Evaluated Using Spectral Inversion. Bull Seismol Soc Am. https://doi.org/10.1785/0120170254

Lin F-CC, Ritzwoller MH, Snieder R (2009) Eikonal tomography: surface wave tomography by phase front tracking across a regional broad-band seismic array. Geophys J Int 177:1091–1110. https://doi.org/10.1111/j.1365-246X.2009.04105.x

Lin W, Doan ML, Moore JC, Mcneill L, Byrne T, Ito T, Saffer D, Conin M, Kinoshita M, Sanada Y, Moe KT, Araki E, Tobin H, Boutt D, Kano Y, Hayman NW, Flemings P, Huftile G, Cukur D, Buret C, Schleicher A, Efimenko N, Kawabata K, Buchs D, Jiang S, Kameo K, Horiguchi K, Wiersberg T, Kopf A, Kitada K et al (2010) Present-day principal horizontal stress orientations in the Kumano forearc basin of the southwest Japan subduction zone determined from IODP NanTroSEIZE drilling site C0009. Geophys Res Lett 37. https://doi.org/10.1029/2010GL043158

Meier U, Shapiro NM, Brenguier F (2010) Detecting seasonal variations in seismic velocities within Los Angeles basin from correlations of ambient seismic noise. Geophys J Int 181:985–996. https://doi.org/10.1111/j.1365-246X.2010.04550.x

Minato S, Tsuji T, Ohmi S, Matsuoka T (2012) Monitoring seismic velocity change caused by the 2011 Tohoku-oki earthquake using ambient noise records. Geophys Res Lett 39. https://doi.org/10.1029/2012GL051405

Miyazaki S, Heki K (2001) Crustal velocity field of southwest Japan: subduction and arc-arc collision. J Geophys Res Solid Earth 106:4305–4326. https://doi.org/10.1029/2000JB900312

Moore GF, Park JO, Bangs NL, Gulick SP, Tobin HJ, Nakamura Y, Sato S, Tsuji T, Yoro T, Tanaka H, Uraki S, Kido Y, Sanada Y, Kuramoto S, Taira A (2009) Structural and seismic stratigraphic framework of the NanTroSEIZE stage 1 transect. Proc IODP 314:315–316. https://doi.org/10.2204/iodp.proc.314315316.102

Nakano M, Hori T, Araki E, Kodaira S, Ide S (2018) Shallow very-low-frequency earthquakes accompany slow slip events in the Nankai subduction zone. Nat Commun 9:984. https://doi.org/10.1038/s41467-018-03431-5

Nakano M, Nakamura T, Kamiya S, Kaneda Y (2014) Seismic activity beneath the Nankai trough revealed by DONET ocean-bottom observations. Mar Geophys Res 35:271–284. https://doi.org/10.1007/s11001-013-9195-3

Nakano M, Nakamura T, Kamiya S, Ohori M, Kaneda Y (2013) Intensive seismic activity around the Nankai trough revealed by DONET ocean-floor seismic observations. Earth, Planets Sp 65:5–15. https://doi.org/10.5047/eps.2012.05.013

Nakata N, Chang JP, Lawrence JF, Boué P (2015) Body wave extraction and tomography at Long Beach, California, with ambient-noise interferometry. J Geophys Res Solid Earth 120:1159–1173. https://doi.org/10.1002/2015JB011870

Nakata N, Snieder R, Tsuji T, Larner K, Matsuoka T (2011) Shear wave imaging from traffic noise using seismic interferometry by cross-coherence. Geophysics 76:SA97–SA106. https://doi.org/10.1190/geo2010-0188.1

Nimiya H, Ikeda T, Tsuji T (2017) Spatial and temporal seismic velocity changes on Kyushu Island during the 2016 Kumamoto earthquake. Sci Adv 3:e1700813. https://doi.org/10.1126/sciadv.1700813

Obermann A, Froment B, Campillo M, Larose E, Planès T, Valette B, Chen JH, Liu QY (2014) Seismic noise correlations to image structural and mechanical changes associated with the Mw 7.9 2008 Wenchuan earthquake. J Geophys Res Solid Earth 119:3155–3168. https://doi.org/10.1002/2013JB010932

Obermann A, Planès T, Larose E, Campillo M (2013) Imaging preeruptive and coeruptive structural and mechanical changes of a volcano with ambient seismic noise. J Geophys Res Solid Earth 118:6285–6294. https://doi.org/10.1002/2013JB010399

Park J-O, Fujie G, Wijerathne L, Hori T, Kodaira S, Fukao Y, Moore GF, Bangs NL, Kurumoto S, Taira A (2010) A low-velocity zone with weak reflectivity along the Nankai subduction zone. Geology 38:283–286. https://doi.org/10.1130/G30205.1

Rubinstein JL, Beroza GC (2004) Evidence for widespread nonlinear strong ground motion in the M_W 6.9 Loma Prieta earthquake. Bull Seismol Soc Am 94:1595–1608. https://doi.org/10.1785/012004009

Seno T, Stein S, Gripp AE (1993) A model for the motion of the Philippine Sea plate consistent with NUVEL-1 and geological data. J Geophys Res Solid Earth 98:17941–17948. https://doi.org/10.1029/93JB00782

Sens-Schönfelder C, Wegler U (2006) Passive image interferometry and seasonal variations of seismic velocities at Merapi Volcano, Indonesia. Geophys Res Lett 33:L21302. https://doi.org/10.1029/2006GL027797

Shapiro NM, Campillo M, Stehly L, Ritzwoller MH (2005) High-resolution surface-wave tomography from ambient seismic noise. Science 307:1615–1618. https://doi.org/10.1126/science.1108339

Shapiro SA (2003) Elastic piezosensitivity of porous and fractured rocks. Geophysics 68:482–486. https://doi.org/10.1190/1.1567215

Suzuki K, Nakano M, Takahashi N, Hori T, Kamiya S, Araki S, Nakata R, Kaneda Y (2016) Synchronous changes in the seismicity rate and ocean-bottom hydrostatic pressures along the Nankai trough: a possible slow slip event detected by the Dense Oceanfloor Network system for Earthquakes and Tsunamis (DONET). Tectonophysics 680:90–98. https://doi.org/10.1016/j.tecto.2016.05.012

Taira T, Brenguier F (2016) Response of hydrothermal system to stress transients at Lassen Volcanic Center, California, inferred from seismic interferometry with ambient noise. Earth Planets Sp 68:162. https://doi.org/10.1186/s40623-016-0538-6

Taira T, Brenguier F, Kong Q (2015) Ambient noise-based monitoring of seismic velocity changes associated with the 2014 Mw 6.0 South Napa earthquake. Geophys Res Lett 42:6997–7004. https://doi.org/10.1002/2015GL065308

Taira T, Nayak A, Brenguier F, Manga M (2018) Monitoring reservoir response to earthquakes and fluid extraction, Salton Sea geothermal field, California. Sci Adv 4:e1701536. https://doi.org/10.1126/sciadv.1701536

Tobin HJ, Saffer DM (2009) Elevated fluid pressure and extreme mechanical weakness of a plate boundary thrust, Nankai Trough subduction zone. Geology 37:679–682. https://doi.org/10.1130/G25752A.1

Toh A, Obana K, Araki E (2018) Distribution of very low frequency earthquakes in the Nankai accretionary prism influenced by a subducting-ridge. Earth Planet Sci Lett 482:342–356. https://doi.org/10.1016/j.epsl.2017.10.062

Toksöz MN, Cheng CH, Timur A (1976) Velocities of seismic waves in porous rocks. GEOPHYSICS 41:621–645. https://doi.org/10.1190/1.1440639

Tonegawa T, Fukao Y, Takahashi T, Obana K, Kodaira S, Kaneda Y (2015) Ambient seafloor noise excited by earthquakes in the Nankai subduction zone. Nat Commun 6:6132. https://doi.org/10.1038/ncomms7132

Tsuji S, Yamaoka K, Ikuta R, Watanabe T, Katsumata A, Kunitomo T (2016) Seismic velocity change in Tokai region detected by Morimachi ACROSS. In: Japan Geoscience Union Meeting

Tsuji T, Ashi J, Strasser M, Kimura G (2015) Identification of the static backstop and its influence on the evolution of the accretionary prism in the Nankai Trough. Earth Planet Sci Lett 431:15–25. https://doi.org/10.1016/j.epsl.2015.09.011

Tsuji T, Dvorkin J, Mavko G, Nakata N, Matsuoka T, Nakanishi A, Kodaira S, Nishizawa O (2011) V P / V S ratio and shear-wave splitting in the Nankai

Trough seismogenic zone: insights into effective stress, pore pressure, and sediment consolidation. Geophysics 76:WA71–WA82. https://doi.org/10.1190/1.3560018

Tsuji T, Kamei R, Pratt RG (2014) Pore pressure distribution of a mega-splay fault system in the Nankai Trough subduction zone: insight into up-dip extent of the seismogenic zone. Earth Planet Sci Lett 396:165–178. https://doi.org/10.1016/j.epsl.2014.04.011

Tsuji T, Minato S, Kamei R, Tsuru T, Kimura G (2017) 3D geometry of a plate boundary fault related to the 2016 Off-Mie earthquake in the Nankai subduction zone, Japan. Earth Planet Sci Lett 478:234–244. https://doi.org/10.1016/j.epsl.2017.08.041

Tsuji T, Tokuyama H, Costa Pisani P, Moore G (2008) Effective stress and pore pressure in the Nankai accretionary prism off the Muroto Peninsula, southwestern Japan. J Geophys Res Solid Earth 113:1–19. https://doi.org/10.1029/2007JB005002

Wallace LM, Araki E, Saffer D, Wang X, Roesner A, Kopf A, Nakanishi A, Power W, Kobayashi R, Kinoshita C, Toczko S, Kimura T, Machida Y, Carr S (2016) Near-field observations of an offshore M w 6.0 earthquake from an integrated seafloor and subseafloor monitoring network at the Nankai Trough, Southwest Japan. J Geophys Res Solid Earth 121:8338–8351. https://doi.org/10.1002/2016JB013417

Wang K, Hu Y (2006) Accretionary prisms in subduction earthquake cycles: the theory of dynamic Coulomb wedge. J Geophys Res Solid Earth 111:B06410. https://doi.org/10.1029/2005JB004094

Wang Q-Y, Brenguier F, Campillo M, Lecointre A, Takeda T, Aoki Y (2017) Seasonal crustal seismic velocity changes throughout Japan. J Geophys Res Solid Earth 122:7987–8002. https://doi.org/10.1002/2017JB014307

Weaver RL, Hadziioannou C, Larose E, Campillo M (2011) On the precision of noise correlation interferometry. Geophys J Int 185:1384–1392. https://doi.org/10.1111/j.1365-246X.2011.05015.x

Wessel P, Smith WHF (1998) New, improved version of generic mapping tools released. EOS Trans Am Geophys Union 79:579–579. https://doi.org/10.1029/98EO00426

Wu C, Peng Z, Ben-Zion Y (2009) Non-linearity and temporal changes of fault zone site response associated with strong ground motion. Geophys J Int 176:265–278. https://doi.org/10.1111/j.1365-246X.2008.04005.x

Yamaoka K, Kunitomo T, Miyakawa K, Kobayashi K, Kumazawa M (2008) A trial for monitoring temporal variation of seismic velocity using an ACROSS system. Island Arc 10:336–347. https://doi.org/10.1111/j.1440-1738.2001.00332.x

Yokota Y, Ishikawa T, Watanabe S, Tashiro T, Asada A (2016) Seafloor geodetic constraints on interplate coupling of the Nankai Trough megathrust zone. Nature 534:374–377. https://doi.org/10.1038/nature17632

Zinszner B, Johnson PA, Rasolofosaon PNJ (1997) Influence of change in physical state on elastic nonlinear response in rock: significance of effective pressure and water saturation. J Geophys Res Solid Earth 102:8105–8120. https://doi.org/10.1029/96JB03225